Twelfth Australasian Fluid Mechanics Conference
The University of Sydney, Australia 1995

EFFECTS OF SECONDARY FLOWS ON DEVELOPING, TURBULENT ROTATING BOUNDARY LAYERS.

Ian Macfarlane and Peter N. Joubert
Department of Mechanical and Manufacturing Engineering
The University of Melbourne
Parkville, Victoria
AUSTRALIA

ABSTRACT

The work presented in this paper represents part of an experimental investigation into the interaction of secondary flows with rotating turbulent boundary layers developing in a zero pressure gradient flow. Results are presented for a radial duct of three aspect-ratios: *ar4* (4:1, height:width), *ar2* (2:1) and *ar1* (1:1). The *ar4* and *ar2* cases show little effect of secondary flows on the midspan mean flow parameters. The *ar1* case shows the secondary flows are strongly influencing the boundary layer development.

INTRODUCTION

Although there have been a number of reports presented on the effect of system rotation on developing turbulent boundary layers, due to the complex nature of such flows, there remains a need for good experimental data to aid our understanding in this area.

The secondary cross flows (Ekman layer flows) are generated by an imbalance between the Coriolis force and pressure force acting on the slower moving particles at the top and bottom walls of the rotating duct. This imbalance deflects fluid from the pressure side toward the suction side, generating the secondary flows. The effect of this on the side wall boundary layers is opposite to that of the Coriolis instability alone.

There have been several experimental investigations in high aspect-ratio experimental rigs. In this case the secondary flows are sufficiently removed from the mid-span boundary layers to allow study of the Coriolis instability in isolation from the Ekman layers. There have also been several studies in low aspect-ratio ducts, where the secondary flow effects dominate the boundary layer development. The current study investigates the intermediate aspect-ratios and evaluates when the secondary flow effects begin to govern the flow.

The boundary layer development observed by Watmuff, Witt and Joubert (1985) in their zero pressure gradient rotating duct was for suction side layer growth to be suppressed while the pressure side layers were enhanced compared with the zero rotation case. The aspect-ratio of the duct used in these experiments was 4:1 (height:width).

Hill and Moon (1962) and Moon (1964) studied the effects of system rotation on developing turbulent boundary layers on the side wall of low aspect-ratio rotating rectangular channels. The measurements showed that boundary layer growth was promoted on the suction side while suppressed on the pressure side. This is in agreement with the conclusions of the preliminary report presented by Koyama et al.(1989) who were conducting experiments in a 1:7 (h:w) low aspect-ratio rotating channel. This is contrary to the findings of Watmuff et al. (1985).

The explanation for the differing trends observed in boundary layer growth mentioned above is that for the higher aspect-ratio experimental rigs, the secondary flow effects are sufficiently removed from the centre line velocity profiles to provide negligible influence. In the lower aspect-ratios, the secondary flows are sufficiently close to the centre line profiles to overcome the Coriolis instability. The above studies have been performed in isolation and to date there has been no studies conducted which provide direct comparison of results with differing secondary flow effects on developing turbulent boundary layers.

Moore (1967) investigated the relative importance of the Coriolis instability and the large scale secondary circulations on fully developed turbulent duct flow. He found mid span velocity and turbulence profiles to be significantly effected by the secondary flows

in aspect-ratios of $\frac{1}{2}:1$ and 1:1, while 4:1 and $7\frac{1}{2}:1$ were little affected.

EXPERIMENTAL SET-UP

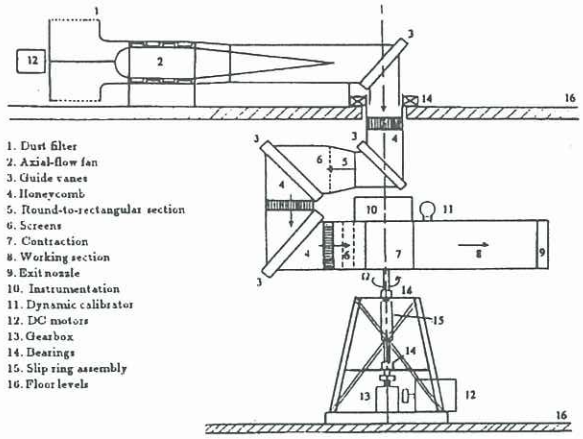

Figure 1: Elevation of rotating wind tunnel

The open return tunnel used in the experiments is shown in figure 1. Air flow was provided by a two stage axial fan located on the floor above the rotating assembly. The air passed through rotating ductwork fitted with turning vanes, honeycombs and screens to ensure that the flow was approximately irrotational relative to the duct at the working section entry. Care has been taken to ensure the working section boundary layers are two dimensional in the zero rotation case. 240 volt power, control and data signals were all provided to the rotating rig through high quality slip rings. Data signals were all amplified prior to transmission through the slip rings to maximise signal-to-noise ratio.

Figure 2 shows an isometric sketch of the working section. It defines the coordinate system used and the pressure and suction side walls for the direction of rotation shown. The full working section was used for $ar4$. Two plates were fitted into the working section, symmetrically about the centre line to provide the reduced aspect-ratios. The plates extended upstream approximately 75mm into the contraction.

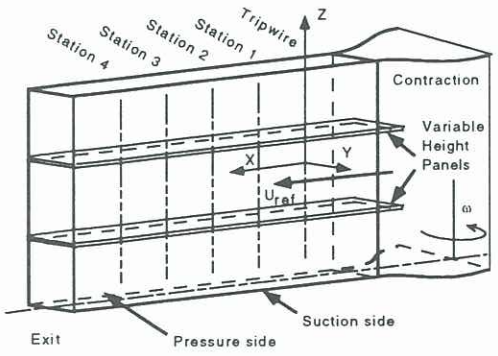

Figure 2: Isometric view of working section.

The free stream turbulence intensity at the working section entrance was less than 0.15% for stationary cases and 0.35% with rotation. A stepping motor traverse mechanism mounted on one side of the working section traversed probes through the boundary layer on the opposite wall. In order to study pressure and suction side behaviour, the direction of tunnel rotation was reversible. Positive rotation corresponded to the pressure side and negative to the suction side. The pressure gradient C_p for all aspect-ratios was adjusted to within $\pm 0.5\%$ stationary case. C_p was not significantly affected by rotation.

To allow for daily variation in temperature and pressure, the tunnel velocity was set to a unit Reynolds number of $Re_{ref} = \frac{U}{\nu} = 664,000 \pm 0.5\%$. This corresponded to a nominal reference velocity U_R of $10m/s$. The rotation rate of the tunnel was set to $1Hz$, giving Rossby number range of $Ro_x = \frac{U_R}{\omega X} =$ 1.6 to 5.3. The boundary layers were tripped by a 1.2 mm diameter trip wire.

The spanwise (Z direction) skin friction measurements were made with a 1.0mm diameter preston tube. The value of y^+ for the Preston tube ranged from approximately 30 to 50 for the various cases. The calculation method used for evaluating skin friction was that outlined in Patel (1965).

Centre line meanflow results presented here were measured with a 0.6mm diameter total head tube and a wall static pressure tapping. The method outlined by Johnston et.al. (1972) was used to correct rotating results for the non-linear static pressure variation across the duct. The wall normal distance was corrected to allow for proximity of the total head probe to the wall. The correction used was that of Macmillan (1956).

Most meanflow results were repeated with a normal hot wire anemometer. Results obtained with the two methods generally agreed to better than 2%.

RESULTS

Spanwise Skin Friction

Figures 3 and 4 show the spanwise skin friction distribution measured at station 1 and 4 respectively. Due to the large range of C'_f the values have been non-dimensionalised by the average value of the spanwise traverse, $C'_{f\,m}$. The actual magnitudes of C'_f can be seen in figure 5.

Figure 3 shows the two dimensionality of the zero rotation layers. Variation in C'_f at station 1 is within $\pm 2.5\%$ for the central region of the flow, away from the influence of the top and bottom walls.

Evidence of the well documented longitudinal roll cell pattern can be seen most clearly in figure 4 (a). The pressure side skin friction shows the large spatially periodic variation, corresponding to the longitudinal roll cell pattern. As the aspect-ratio was reduced the roll cell pattern appeared unaffected by secondary flows. The variations in C'_f are very similar both spatially and in magnitude for the regions

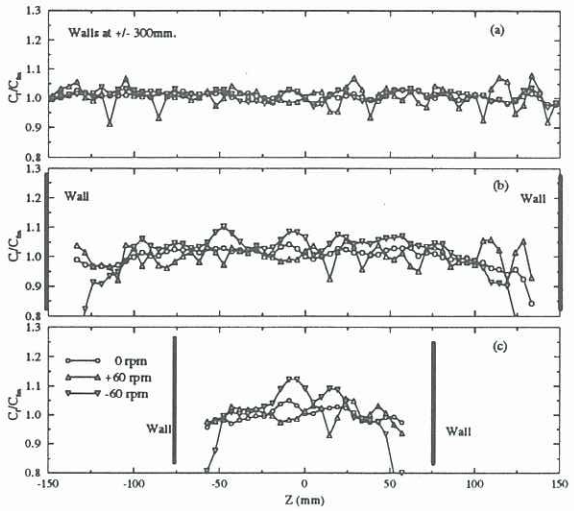

Figure 3: Station 1 spanwise skin friction (a) *ar4*, (b) *ar2*, (c) *ar1*

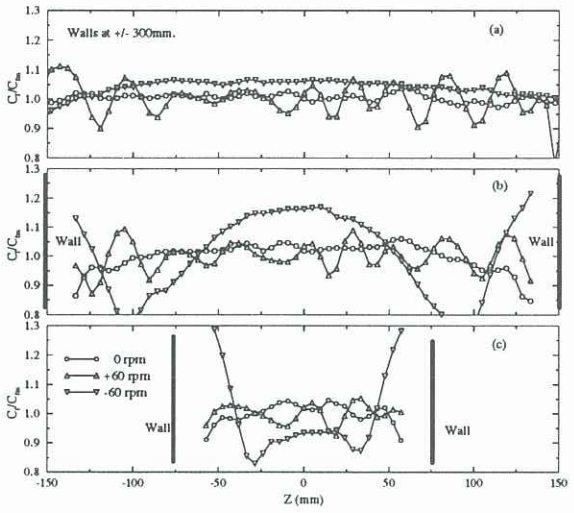

Figure 4: Station 4 spanwise skin friction (a) *ar4*, (b) *ar2*, (c) *ar1*

measured as the aspect-ratio was reduced.

The secondary flow effects can be seen for *ar2* and *ar1* where measurements close to the horizontal boundaries of the working section were possible. The relatively large values of skin friction near the top and bottom walls correspond to the secondary flows moving towards the suction side wall. Then as the flow is turned toward the centre and eventually away from the suction side wall the skin friction decreases. We can see from figure 5 that the magnitude of C_f' at the centre line is very similar between *ar4* and *ar2*. However figure 4 shows that the unaffected region at the centre of the side wall is small and effects of the secondary flows are felt over most of the suction side wall. Figure 4 (c) shows that for *ar1* the secondary flows are dominating the entire suction side wall.

Streamwise Skin Friction

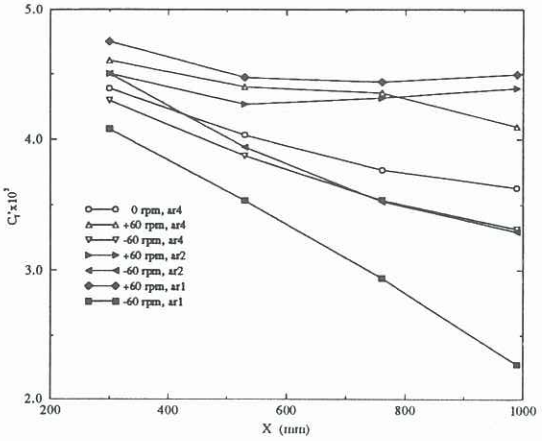

Figure 5: Streamwise skin friction coefficient

Figure 5 shows the streamwise skin friction distribution. The zero rotation results were similar in all cases, so to reduce congestion in the figure only the *ar4* zero rotation result is shown. The plot clearly shows the strong influence of the Ekman layer on the boundary layer for *ar1* with a marked reduction in skin friction on the suction side. The reduction in skin friction on the suction side was also seen in Macfarlane and Joubert (1992). They suggest that low aspect-ratio rotating, diffusing flows would be more susceptible to separation or stall than higher aspect-ratio cases in an otherwise equivalent flow. The differences on the pressure side are much smaller, but show an increase in the skin friction as aspect-ratio is reduced. from *ar2* to *ar1*. The variations between *ar4* and *ar2* are probably due to the large variations in skin friction across the span and the subsequent difficulty of placing the total head probe at a location corresponding to the mean value of C_f'.

Boundary Layer Thickness

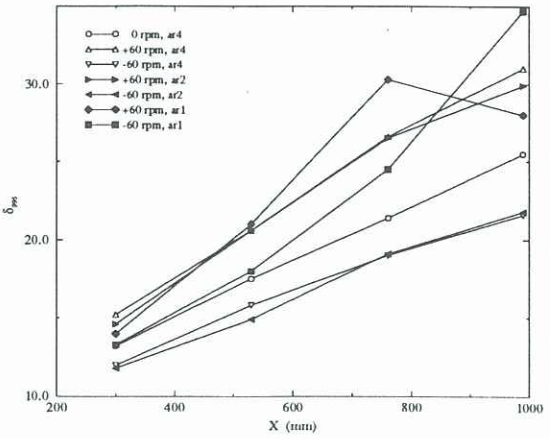

Figure 6: Boundary Layer thickness

Boundary layer growth is shown in figure 6. As for

figure 5, only the *ar4* zero rotation case is shown. The expected trend of growth promoted on the pressure side and suppressed on the suction side due to the influence of the Coriolis instability alone is seen for *ar4*. The *ar2* case shows similar results with very little effect of Ekman layers on the mid span meanflow profiles. The *ar1* case shows significant effects of the Ekman layer. Initially the suction side layer is thicker than for zero rotation with the pressure side thicker again. By station 4 the suction side has grown to be larger than pressure side. Both are still larger than the zero rotation case, although extrapolating the results indicates the pressure side layer would quickly reduce in thickness to less than the zero rotation case with streamwise development.

Meanflow Profiles

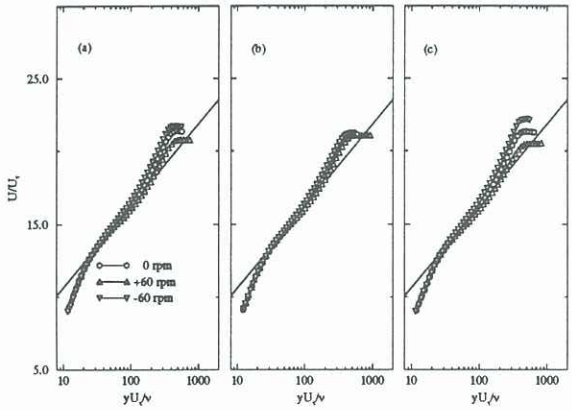

Figure 7: Station 1 Meanflow Profiles (a) *ar4*, (b) *ar2*, (c) *ar1*

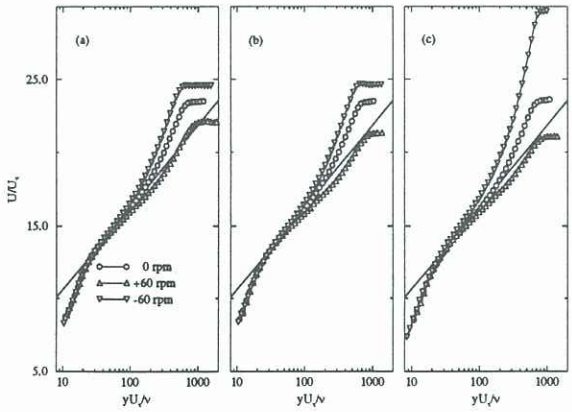

Figure 8: Station 4 Meanflow Profiles (a) *ar4*, (b) *ar2*, (c) *ar1*

Figures 7 and 8 show the boundary layer meanflow profiles plotted in standard non-dimensionalised coordinates for station 1 and 4. The zero rotation layers all fit well with the logarithmic law of the wall. The gradient of the log region is increased on the suction side and decreased on the pressure side. This change of gradient seems unaffected by aspect-ratio and the subsequent influence of secondary flows. A strong influence is seen for *ar1* in the wake region. The wake parameter by observation from the figure is significantly larger for *ar1* suction side layer than for *ar2* or *ar4*. The pressure side wake parameter is slightly reduced.

CONCLUSION

The results presented here show that the pressure side demonstrates relatively small changes in the centre line mean flow parameters and spanwise skin friction between *ar4* and *ar2*. Significant effects are seen in the mid-span parameters, particularly for boundary layer thickness, at *ar1*. By station 4 the boundary layer thickness is significantly reduced.

The suction side is significantly effected by the Ekman layer flow. Effects can be seen on the skin friction away from the centre line at *ar2* and the effects dominate the entire boundary layer by *ar1*. The skin friction results suggest low aspect rotating diffusing flows would be far more susceptible to separation than an equivalent high aspect-ratio case.

REFERENCES

HILL, P. G. and MOON, I. M. (1962) Effects of Coriolis forces on the turbulent boundary layer in rotating machines. Rep. No. 69, Gas Turbine Laboratory, M.I.T..

JOHNSTON, J.P., HALLEEN, R.M. and LEZIUS, D.K. (1972) Effects of rotation on the structure of two-dimensional fully developed turbulent channel flow. J. Fluid Mech., 56, pp. 533-557.

KOYOMA, H. S., TAMURA, E. and SAITO, T. (1989) Effect of Coriolis force on developing channel flow. 10th Australasian Fluid Mechanics Conference, Melbourne Australia, Dec. 11- 15.

MACFARLANE, I and JOUBERT P.N. (1992) Interaction of the Ekman layer and side wall boundary layer with system rotation and adverse pressure gradient. 11th Australasian Fluid Mechanics Conference, Hobart, Australia, Dec. 14- 18.

MACMILLAN, F.A. 1956 Experiments on pitot tubes in shear flows. Aero. Res. Counc. R. & M. 3028.

MOON, I. M. (1964) Effects of Coriolis forces on the turbulent boundary layer in rotating fluid machines. Rep No. 89 Gas Turbine Laboratory, M.I.T..

MOORE, J. (1967) Effects of Coriolis on turbulent flow in rotating channels. Rep. No. 69, Gas Turbine Laboratory, M.I.T..

PATEL, V.C. 1965 Calibration of the Preston tube and limitations on its use in pressure gradients. J. Fluid Mech. 23, 185.

WATMUFF, J. H., WITT, H. T. and JOUBERT, P. N. (1985) Developing turbulent boundary layers with system rotation. J. Fluid Mech., 157, pp. 405-448.